Cement and Concrete Research 40 (2010) 898–907

Contents lists available at ScienceDirect

Cement and Concrete Research

journal homepage: http://ees.elsevier.com/CEMCON/default.asp

Effect of silicate modulus and metakaolin incorporation on the carbonation of alkali silicate-activated slags

Susan A. Bernal [a,*], Ruby Mejía de Gutierrez [a], John L. Provis [b,*], Volker Rose [c]

[a] Materials Engineering Department, Composite Materials Group, CENM, Universidad del Valle, Cali, Colombia
[b] Department of Chemical and Biomolecular Engineering, University of Melbourne, Victoria 3010, Australia
[c] Advanced Photon Source, Argonne National Laboratory, Argonne, Illinois 60439, USA

ARTICLE INFO

Article history:
Received 16 November 2009
Accepted 1 February 2010

Keywords:
Alkali-activated slag (C)
Metakaolin (D)
Silicate modulus (B)
Carbonation (C)
High-resolution X-ray diffraction (B)

ABSTRACT

Accelerated carbonation is induced in pastes and mortars produced from alkali silicate-activated granulated blast furnace slag (GBFS)–metakaolin (MK) blends, by exposure to CO_2-rich gas atmospheres. Uncarbonated specimens show compressive strengths of up to 63 MPa after 28 days of curing when GBFS is used as the sole binder, and this decreases by 40–50% upon complete carbonation. The final strength of carbonated samples is largely independent of the extent of metakaolin incorporation up to 20%. Increasing the metakaolin content of the binder leads to a reduction in mechanical strength, more rapid carbonation, and an increase in capillary sorptivity. A higher susceptibility to carbonation is identified when activation is carried out with a lower solution modulus (SiO_2/Na_2O ratio) in metakaolin-free samples, but this trend is reversed when metakaolin is added due to the formation of secondary aluminosilicate phases. High-energy synchrotron X-ray diffractometry of uncarbonated paste samples shows that the main reaction products in alkali-activated GBFS/MK blends are C–S–H gels, and aluminosilicates with a zeolitic (gismondine) structure. The main crystalline carbonation products are calcite in all samples and trona only in samples containing no metakaolin, with carbonation taking place in the C–S–H gels of all samples, and involving the free Na^+ present in the pore solution of the metakaolin-free samples. Samples containing metakaolin do not appear to have the same availability of Na^+ for carbonation, indicating that this is more effectively bound in the presence of a secondary aluminosilicate gel phase. It is clear that claims of exceptional carbonation resistance in alkali-activated binders are not universally true, but by developing a fuller mechanistic understanding of this process, it will certainly be possible to improve performance in this area.

1. Introduction

Durability is one of most important properties of cementitious materials because it is associated with the life service of civil structures, and is modified by the interaction of the material with the environment. The presence of CO_2 in the atmosphere, including the higher levels now being induced by human-derived CO_2 emissions, affects the long-term durability of built structures through the sequence of degradation phenomena that are jointly referred to as carbonation [1–4]. The mechanism of carbonation consists of diffusion through gas, aqueous and solid/gel binder phases, as well as chemical reaction processes. The overall rate of carbonation is controlled by the physical properties of the solid binder, in particular the porosity and pore size distribution of the material and the CO_2 permeability through the porous network. Gas diffusion is in many situations the slowest step of the overall process [5–7].

The carbonation of Portland cement (OPC) mortar and concrete is a widely studied and well-understood phenomenon. Carbon dioxide in the atmosphere diffuses inside the material and dissolves in the pore water, forming carbonic acid. Carbonic acid may then attack calcium-containing phases, initially the calcium hydroxide and then calcium silicate hydrates (C–S–H) and calcium aluminate hydrates (C–A–H), to form calcium carbonate. This leads, in the long-term, to a reduction of the alkalinity in the cementitious system, accompanied by reduced mechanical performance and the corrosion of steel reinforcement [1–3,5–7].

Under natural environmental conditions the process of carbonation of cementitious materials is a long-term reaction as consequence of the relatively low CO_2 concentration present in the atmosphere (≈0.038% v/v). Therefore, accelerated carbonation testing is often used in order to induce the carbonation of concretes. Castellote et al. [8], using OPC pastes assessed under accelerated carbonation test conditions, have identified that the reaction products formed at a CO_2 concentration of 3% are comparable with those observed in samples carbonated at natural conditions. This indicates that this degree of acceleration of the carbonation process does not

* Corresponding authors. Tel.: +61 3 8344 8755; fax: +61 3 8344 4153.
E-mail addresses: susana.bernal@gmail.com (S.A. Bernal), jprovis@unimelb.edu.au (J.L. Provis).

0008-8846/$ – see front matter © 2010 Elsevier Ltd. All rights reserved.
doi:10.1016/j.cemconres.2010.02.003

introduce new carbonation mechanisms which would not be observed under natural environmental conditions for those materials; the same was not true for CO_2 concentrations of 10% or higher [8].

Several previous studies have examined the carbonation of alkali-activated slag (AAS) and other related alkali-activated binders. Byfors et al. [9] identified that F-concrete (a trade name for a material which used as the binder blast furnace slag activated by a combination of alkali metal compounds) exhibits a higher carbonation rate than Portland cement concrete with the same compressive strength. Bakharev et al. [10] and Puertas et al. [11] also found that alkali silicate- or hydroxide-activated slag mortars and concretes are more rapidly carbonated than comparable OPC mixes, and that this degradation can lead to an important decrease in compressive strength. Those results are coherent with those reported by Palacios et al. [12] and Bernal et al. [13], who suggest that the carbonation mechanism is not the same in Portland and alkali-activated slag cements as consequence of the differences between the reaction products of both systems.

On the other hand, Deja [14] identified a similar carbonation rate in AAS mortars and concretes under service conditions when compared with OPC-based samples. An improvement in the compressive strength with long-term exposure to CO_2 was also reported, and attributed to pore size refinement associated with the deposition of the carbonation reaction products. The previous was more significant in samples activated with $Na_2O{\cdot}rSiO_2$ in contrast to specimens activated with Na_2CO_3. Xu et al. [15], studying aged concretes (up to 35 years) based on slag activated with carbonates or carbonate/hydroxide blends, observed an acceptable carbonation rate of all samples (0.03–0.5 mm/year), proving the high stability of these AAS binders. These results are contrary to the reports of carbonation problems in AAS mortars and concretes as mentioned above [9–13]. It may also be that there is a distinction to draw here between accelerated and in-service conditions, where the accelerated tests seem to influence alkali-activated materials more severely; this will certainly be an area worthy of further study.

Additionally, it is important to note that there are no previous reports in the literature related to the carbonation mechanism or rate of pastes or mortars based on alkali-activated granulated blast furnace slag/metakaolin (GBFS/MK) blends. Such blends are of interest because the combination of the reaction products obtained after the activation of GBFS/MK (coexisting C–S–H and sodium aluminosilicate hydrate (N–A–S–H) gels) has been recognized as a stable system that could exhibit improved durability when compared to binders prepared from a sole raw material [16–18].

In light of such obvious discrepancies in the previous results regarding the carbonation of AAS binders, and the unknown performance of alkali silicate-activated GBFS/MK blends when exposed to this form of chemical attack, the aim of this work is to study the effect of the activator modulus and the presence of metakaolin on the carbonation of pastes and mortars based on these binders.

2. Experimental program

2.1. Materials

The primary raw material used in this investigation was a Colombian granulated blast furnace slag (GBFS) from the factory *Acerías Paz del Río*. The basicity coefficient ($K_b = CaO + MgO/SiO_2 + Al_2O_3$) and the quality coefficient ($CaO + MgO + Al_2O_3/SiO_2 + TiO_2$) based on the chemical composition (Table 1) were 1.01 and 1.92, respectively. Its specific gravity was 2900 kg/m^3 and Blaine fineness was 399 m^2/kg. The particle size range, determined through laser granulometry, was 0.1–74 μm, with a d_{50} of 5 μm.

The metakaolin used was generated in the laboratory by calcination of a Colombian kaolin containing minor quartz and dickite impurities. Calcination was carried out at 700 °C in an air atmosphere, for 2 h. The particle size range of the MK was 1.8–100 μm, with a d_{50} of 13.2 μm and 10% of particles finer than 4 μm.

Table 1
Composition of the GBFS and MK used, from X-ray fluorescence analysis. LOI is loss on ignition at 1000 °C.

Component (mass % as oxide)	GBFS	MK
SiO_2	32.29	50.72
Al_2O_3	16.25	44.63
CaO	42.45	2.69
Fe_2O_3	2.35	–
MgO	2.87	–
Other	1.88	0.94
LOI	1.91	1.02

Alkaline activating solutions of the desired composition were formulated by blending using a commercial sodium silicate solution with 32.4 wt.% SiO_2, 13.5 wt.% Na_2O and 54.1 wt.% H_2O, and 50 wt.% NaOH solution, to reach the desired modulus (SiO_2/Na_2O molar ratio, denoted Ms) of 1.6, 2.0 or 2.4. A constant activator concentration of 5% Na_2O by mass of GBFS + MK was used.

2.2. Sample synthesis and test procedure

2.2.1. Mortars

Mortars were produced following the standard procedure ASTM C305-06 "*Standard Practice for Mechanical Mixing of Hydraulic Cement Pastes and Mortars of Plastic Consistency*". River sand with a fineness modulus of 2.75 was used as fine aggregate. All samples were formulated with a constant water/(GBFS + MK + anhydrous activator) ratio of 0.47 and a binder/sand ratio of 1:2.75. While this is quite a high water content for alkali-activated mortars, it was designed to replicate a binder formulation which has been used successfully in the preparation of AAS concretes [18]. The specimens were cast in cubic moulds with dimensions of 50.8 × 50.8 mm, and stored under controlled humidity (relative humidity (RH) ~85%) and ambient temperature (~25 °C) for 24 h. Samples were then demolded and cured under RH of 90% and a temperature of 27 ± 2 °C for 28 days.

2.2.2. Pastes

Pastes with a constant water/(GBFS + MK + anhydrous activator) ratio of 0.23 were produced in accordance with the standard procedure ASTM C305-06. The specimens were cast in a cylindrical mould and stored in hermetic containers with a relative humidity of 90% and a temperature of 27 ± 2 °C for 28 days.

2.3. Carbonation

An accelerated carbonation testing system was used in order to induce the carbonation of concretes. The conditions used were a CO_2 concentration of 3.0 ± 0.2%, a temperature of 20 ± 2 °C, and RH = 65 ± 5%.

In order to perform the carbonation measurements, the specimens were removed from the chamber after 340 or 540 h of exposure. The depth of carbonation was measured by treating the surface of a freshly cleaved specimen with a 1% solution of phenolphthalein in alcohol. In the uncarbonated part of the specimen, where the mortar was still highly alkaline, purple-red coloration was obtained, while no coloration is observed in the carbonated region. Each reported result represents the average depth of the carbonation measured at eight points, using two replicate samples (four points per sample). The properties of uncarbonated samples after 28 days of curing are used as reference values, indicated as zero hours of exposure.

Carbonated and uncarbonated mortars were tested following the standard procedure ASTM C 109/C, *Standard Test Method for Compressive Strength of Hydraulic Cement Mortars (using 2-in. or [50-mm] Cube*

Specimens) to determine their compressive strength. Capillary sorptivity, applying the standard procedure EMPA–SIA 162/1 [19], was assessed at different times of CO_2 exposure.

Pastes of the Ms 2.0 and 2.4 mixes were milled and sieved to a particle size of 0.074 mm after 28 days of curing and exposed to CO_2 under the same environmental conditions applied to the mortar specimens. After 1000 h of exposure, samples were tested using the phenolphthalein indicator to ensure that carbonation was complete, and then analyzed:

- X-ray diffractometry was carried out using a high-resolution high-throughput synchrotron powder X-ray diffractometer with a system of twelve simultaneous analyzer/detectors at beamline 11-BM at the Advanced Photon Source (APS), Argonne National Laboratory (USA). The tests were conducted in accordance with the standard protocols for automated data acquisition on the 11-BM beamline. The conditions for the data collection were: continuous scanning of a detector covering an angular range of 34° with a step rate of 0.01°/s, a step size of 0.001° and wavelengths of $\lambda = 0.401738$ Å for uncarbonated samples and 0.458879 Å for carbonated samples. Data have been converted to Q units ($Q = \frac{4\pi \sin\theta}{\lambda}$) for presentation here, to enable more ready comparison between data sets collected at different wavelengths.
- Fourier transform infrared (FTIR) spectrometry was conducted via the KBr pellet technique, using a Shimadzu FTIR 8400 instrument, scanning from 4000 to 400 cm^{-1}.
- A thermogravimeter SDT-Q600 was used to analyze crushed samples, in a nitrogen atmosphere, from 25 to 1100 °C at a heating rate of 10 °C/min.

The samples with Ms 1.6 were not subjected to detailed instrumental analysis, because their mechanical properties were observed to be poor and the paste mixes were unworkable and tended to crack severely.

3. Results and discussion

3.1. Carbonation depth

The incorporation of MK into the binder formulations studied here leads to an increase in the carbonation susceptibility of the AAS mortars (Table 2). Mortars based solely on GBFS activated with a modulus of solution (Ms = ratio SiO_2/Na_2O) of 2.4 show the lowest carbonation depths of all samples studied after 340 h of CO_2 exposure, while every sample was fully carbonated after 540 h. The high water/binder ratio used in the samples will have contributed to this rapid carbonation, and given that the primary aim of this study is to identify carbonation mechanisms and trends rather than to develop a highly carbonation-resistant sample formulation, this is not considered to be problematic.

The trends with respect to activator silicate modulus are somewhat more complex. In the AAS system with no MK added, carbonation rates increase with increasing alkalinity (decreasing modulus), with the Ms = 1.6 sample showing the most rapid carbonation. However, mortars with a GBFS/(GBFS + MK) ratio of 0.9 exhibited the opposite trend in carbonation depth when compared with samples based solely on GBFS. In this case it is observed that reducing Ms gives a slight decrease in the carbonation depth. This suggests that, because decreasing Ms leads to an increase of the system alkalinity, there is a greater potential for MK dissolution and the formation of secondary (probably aluminosilicate) phases that could slow the carbonation process, either by chemical (carbonate-binding) or microstructural means.

Table 2
Carbonation depth of alkali silicate-activated GBFS/MK mortars, expressed as percentage progress of the carbonation front towards the centre of the 50.8 mm mortar blocks as measured at the midpoint of each face.

GBFS/(GBFS + MK) ratio	Carbonation (%)					
	340 h			540 h		
	Ms = 2.4	Ms = 2.0	Ms = 1.6	Ms = 2.4	Ms = 2.0	Ms = 1.6
1.0	61	66	73	100	100	100
0.9	89	80	77	100	100	100
0.8	100	100	100	100	100	100

3.2. Compressive strength

Uncarbonated mortars formulated with alkali-activated GBFS exhibit compressive strengths of up to 67 MPa, with higher strengths achieved using high-modulus activators (Fig. 1). After 540 h of CO_2 exposure, compressive strength values decrease by approximately 60%. However, it is important to highlight that some of the completely carbonated mortars (Ms 2.4 and 2.0) reported residual compressive strengths up to 38 MPa. Such a value of residual strength would be considered sufficient in terms of mechanical behavior for a building material in several civil engineering applications, but corrosion of steel reinforcing would need to be monitored carefully in such cases. It is also interesting to note that the carbonation depths and rates of strength decrease in Table 2 and Fig. 1 do correlate quite well; in general, fully-carbonated samples do not appear to be further degraded by longer-term exposure to CO_2.

The relatively poor performance of mortars activated with the lowest Ms value (1.6) can be attributed to the increased drying shrinkage associated with the very short setting times identified in this mix, with a correspondingly low degree of binder formation [18]. This phenomenon contributes to the ingress of aggressive agents, increasing susceptibility to degradation by transport mechanisms, and also leads to the formation of microcracks in the material, reducing its mechanical performance [20].

Increasing the MK content in the binder to 20% causes significant reductions in the compressive strengths of the uncarbonated mortars, this suggests that the activation conditions might not be conducive to the complete reaction of the MK incorporated in the system. Previous compressive strength data for alkali silicate-activated GBFS/MK blends have shown differences in strength performance with increasing MK addition, depending on the extent of substitution and the activator modulus; the factors controlling this are not yet well understood [17]. However, the susceptibility to carbonation processes in terms of mechanical behavior degradation (percentage strength loss) is not as high as in the other systems studied. Samples exposed to CO_2 over 540 h exhibited decreases in strength of less than 40% (and as low as 12% for the Ms = 1.6 sample) relative to uncarbonated samples.

3.3. Capillary sorptivity

Capillary sorptivity curves obtained after different times of CO_2 exposure are shown in Fig. 2. It can be seen that the progress of carbonation, associated with longer periods of CO_2 exposure, modifies the capillary water absorption properties of the samples — but similar to the mechanical strength performance, samples that are already fully carbonated do not show further changes in sorptivity with more extended exposure to CO_2.

Uncarbonated mortars (0 h) formulated solely with GBFS do not show significant variations in the amount of absorbed water under different activation conditions; however, with exposure to CO_2, the water saturation point of the samples moves to lower times, which indicates a substantial increase in the porosity of the material as a result of the carbonation process, probably due at least in part to the breakdown of C–S–H to form phases which do not chemically bind the

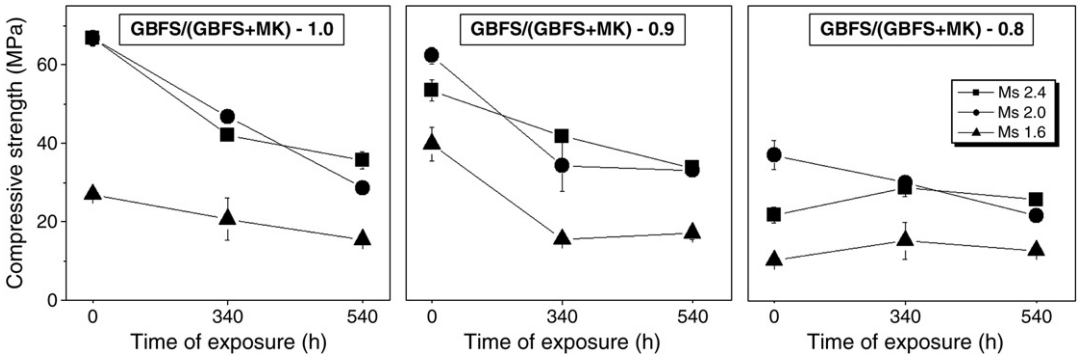

Fig. 1. Compressive strengths of mortars based on alkali-activated GBFS/MK blends as function of GBFS/ (GBFS + MK) ratio and modulus of solution (Ms). Error bars represent one standard deviation, and where not shown are smaller than the data symbols.

same volume of water, and thus the rapid ingress of water early in the test.

After 340 h of CO_2 exposure, the slag-only samples activated with Ms = 1.6 exhibited the highest increase in absorbed water. However, longer exposure times (540 h) led to a reduction in the total amount of water absorbed by almost all samples when compared to 340 h of CO_2 exposure. This is most likely a consequence of the carbonation products becoming deposited in the pore space of the samples. In general, it can be recognized that increasing Ms in the activation process of GBFS/MK blends leads to lower capillary sorptivity in the mortars.

Early in the test, all uncarbonated mortars (0 h) formulated with a GBFS/(GBFS + MK) ratio of 0.9 show comparable amounts of absorbed water. After reaching the saturation point, mortars activated with Ms of 2.0 show the lowest water absorption. The exposure to CO_2 has a similar effect in water saturation point of these mortars when

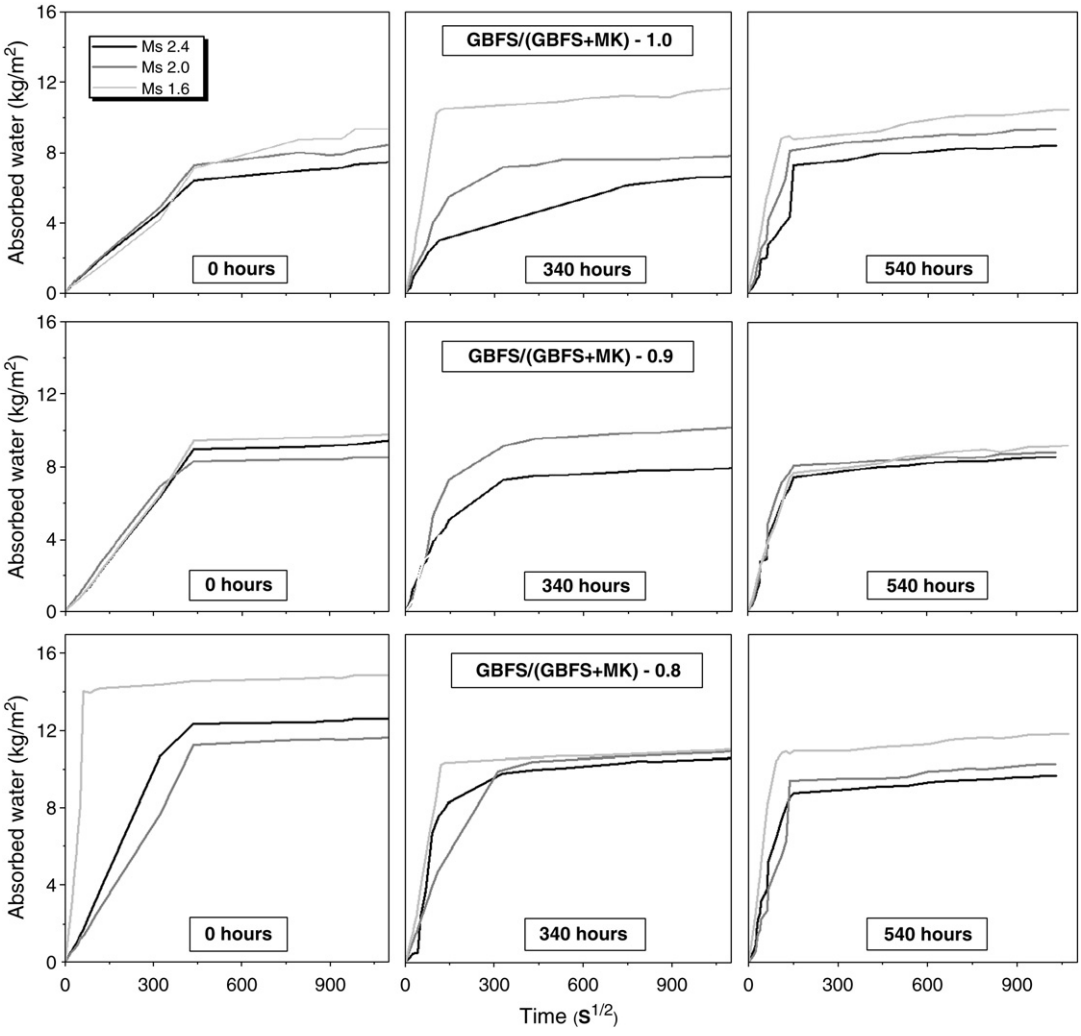

Fig. 2. Capillary sorptivity of alkali-activated GBFS/MK mortars before and after CO_2 exposure.

compared with the slag-only samples. It is also possible to observe that after complete carbonation (540 h), the reduction in water sorptivity is more significant than in mortars without MK.

Carbonated and uncarbonated mortars with GBFS/(GBFS + MK) = 0.8 show a higher absorption of water than the corresponding mortars with lower contents of MK, and uncarbonated samples (0 h) absorb more water than carbonated samples. This performance is coherent with the reduced compressive strength exhibited by these mortars and their increased susceptibility to carbonation — and specimens activated with Ms of 1.6 show the greatest capillary sorptivity, which could be a consequence of the shrinkage observed after preparation as mentioned above.

The kinetics of the capillary sorptivity of mortars can be described by the capillary absorption coefficient (k) and the resistance to water penetration (m), both determined from the capillary sorptivity curves as recommended by Fagerlund [19]. Table 3 shows that k (the initial slope of the sorptivity plots in Fig. 2) increases with the time of exposure to CO_2, this effect being the most significant in samples formulated with GBFS/(GBFS + MK) ratios of 1.0 and 0.9, and activated with a Ms of 1.6. The opposite was observed in samples with a GBFS/(GBFS + MK) ratio of 0.8, where the specimens activated with Ms = 1.6 exhibited a reduction in k of up to 60% at 340 h of carbonation.

In AAS mortars, it has been reported that carbonation leads to a change in the size pore distribution, with a substantial increase in the volume of pores between 1 and 10 μm and a reduction in the range 0.1–1 μm [11–13,21]. This leads to an increase in the average size of pores, and sometimes also (but not in the results presented in Fig. 2) in the total porosity of the material. That behavior has been attributed to a reduced matrix density as a result of the decalcification of the C–S–H gels via reaction with the HCO_3^- formed in the pore solution by the dissolution of CO_2. In addition to the chemical reactions that take place during carbonation, Shi [22] suggests that the carbonation reactions in these materials induce shrinkage, which generates microcracking of the samples and therefore an increase in open and total porosity. These combined phenomena can then contribute to the rapid ingress of the aggressive agent into the material, accelerating its degradation process.

With regard to the resistance to water penetration (Fig. 3; calculated according to the method of Fagerlund [19]: $m = \left(\frac{\text{saturation point}}{k \times \text{sample diameter}}\right)^2$, with saturation point in kg/m^2 and diameter in metres), mortars with GBFS/(GBFS + MK) ratios of 1.0 and 0.9 show a substantial reduction in m upon exposure to CO_2. This indicates a decreased resistance to the total ingress of aggressive agents into the material — the carbonated samples absorb water more rapidly (higher k values with similar saturation points) due to the larger mean pore size and increased microcracking. On the other hand, in mortars with a GBFS/(GBFS + MK) ratio of 0.8, a slight increase in the m value after 540 h of carbonation is identified. These results are also coherent with the trends previously identified in the capillary sorptivity curves and the k values.

Table 3
Capillary sorptivity coefficients of alkali-activated GBFS/MK mortars after exposure to CO_2.

GBFS/ (GBFS + MK) ratio	Ms	k (kg m^{-2} s$^{-1/2}$)		
		0 h	340 h	540 h
1.0	2.4	0.014	0.023	0.038
	2.0	0.012	0.026	0.058
	1.6	0.013	0.046	0.080
0.9	2.4	0.020	0.023	0.053
	2.0	0.022	0.047	0.058
	1.6	0.020	0.031	0.117
0.8	2.4	0.034	0.051	0.072
	2.0	0.024	0.041	0.052
	1.6	0.158	0.063	0.120

These results therefore indicate that the incorporation of MK as a secondary raw material in the binder leads to an increase in the capillary sorptivity of the mortars, which may be a contributing factor in the increased susceptibility to carbonation of these mortars.

3.4. High-energy synchrotron X-ray diffraction

Uncarbonated samples activated with Ms = 2.4 (Fig. 4A) contain, in addition to the major X-ray amorphous phase: gehlenite ($Ca_2Al_2SiO_7$) (Powder Diffraction File (PDF) card 00-035-0755), quartz (SiO_2) (PDF #01-078-2315) and calcite ($CaCO_3$) (PDF# 01-072-1214), attributed to the unreacted GBFS. Two crystalline reaction products have been identified as well: a calcium silicate hydrate (C–S–H) ($Ca_6Si_3O_{12}\cdot xH_2O$) (PDF# 00-014-0035) and the aluminosilicate zeolite gismondine ($CaAl_2Si_2O_8\cdot 4H_2O$) (PDF# 00-020-0452). There do not appear to be any crystalline sodium-containing phases formed; the Na^+ present must therefore either be present in pore solutions or in non-crystalline reaction products. The phases identified in this system are in accordance with those reported by other studies [23–32] when GBFS is activated with sodium silicate solutions, except that gismondine has only once previously been observed in such systems, and then tentatively identified as a transient phase present for a short period during curing [33]. In fact, it is only able to be identified in the current study due to the extremely high resolution of the synchrotron X-ray diffractometer used; the peaks assigned to this phase are small but sharp, and would be difficult to distinguish in most laboratory X-ray diffraction experiments. Sodium-containing zeolites of the gismondine group (zeolite Na-P1 and Na-P2) are very often observed in the alkaline activation of fly ashes, but the identification of this framework type in high-calcium systems such as those studied here is rare.

It is important, therefore, to highlight the nanostructural differences between the reaction products of these binders and of OPC cements. In these alkali-activated binders, portlandite ($Ca(OH)_2$) and ettringite, two of the main reaction products of OPC [34], are not identified. Ettringite would not be expected, as there is no gypsum added as a source of sulfate ions, and the use of high-silica activating solutions precludes the formation of $Ca(OH)_2$, as has been observed in other alkali-activated binder systems [35]. This further highlight the expectation that the carbonation reaction sequence in these binders will progress by mechanisms different from those identified in conventional cements [11–13].

It has previously been indicated that alkali-activated GBFS binders present the possibility to obtain C–S–H gels with some degree of substitution of silicon by aluminum, as well as the potential formation of phases rich in aluminum [12,28,32,36,37]; however, in this study it is clearly identified that an aluminosilicate with the gismondine (zeolite Ca–P) structure is formed in this system. Similar phases have been identified previously in alkali-activated binders based on fly ash [38–40] which are considered to be “zeolite precursors” [38,41]. The observation of gismondine in these samples indicates that binders synthesize by alkali-silicate activation of GBFS and GBFS/MK blends also contain at least some phases which can be considered to be zeolitic precursors. This is consistent with some of the arguments which have been presented by Glukhovsky and colleagues [42], although they more commonly identify sodium-containing zeolite phases such as analcime in their heat-cured AAS specimens.

After carbonation (Fig. 4B), a reduction of the amorphous phase content of the samples is observed, as indicated by changes in the broad feature around $Q = 4$ Å^{-1}. In this case, calcium silicate hydrate (C–S–H) ($Ca_6Si_3O_{12}\cdot xH_2O$) (PDF# 00-0014-0035), calcium aluminosilicate (gismondine) ($CaAl_2Si_2O_6\cdot 4H_2O$) (PDF# 00-020-0452) and quartz (SiO_2) (PDF# 01-078-2315) are identified. As consequence of carbonation, an increase in the intensity of the characteristic peaks of calcite ($CaCO_3$) (PDF# 01-072-1214) relative to the uncarbonated

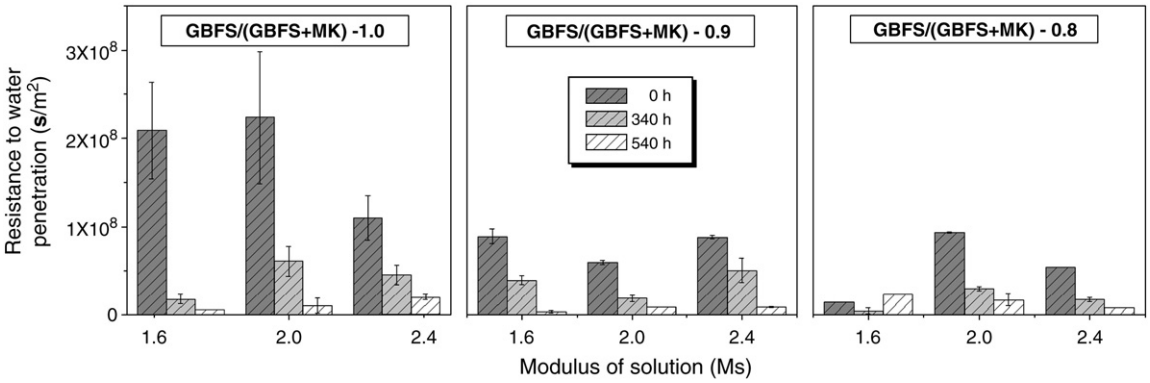

Fig. 3. Water penetration resistance (m) of mortars of alkali-activated GBFS/MK blends as function of GBFS/(GBFS + MK) ratio.

samples is observed. This indicates that calcite is the main carbonation product formed in this system, coherent with data reported by other researchers [11–13]. As a second carbonation product in the slag-only sample, trona ($Na_3H(CO_3)_2 \cdot H_2O$) (PDF #00-029-1447) was also identified. In binders with GBFS/(GBFS + MK) = 0.9, trona was not identified as a carbonation product.

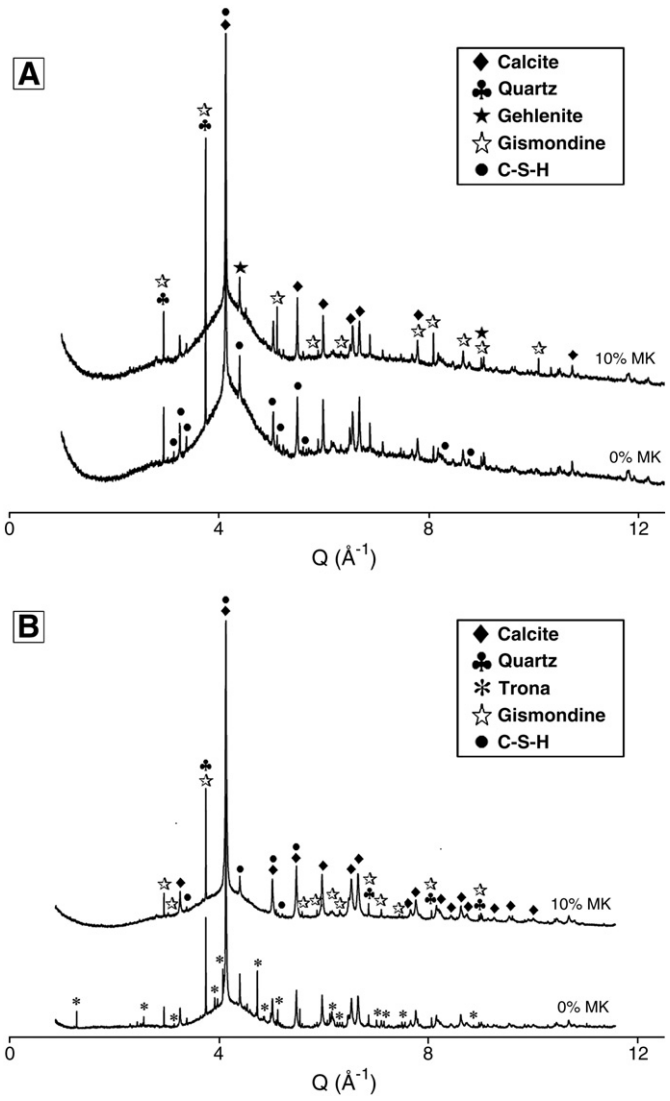

Fig. 4. High resolution synchrotron X-ray diffraction patterns of (A) uncarbonated (λ = 0.401738 Å and (B) carbonated pastes (λ = 0.458879 Å) based on alkali-activated GBFS and GBFS/MK blends with Ms = 2.4.

The preceding results differ from those reported in other studies [11,12] where the main carbonation products have been identified as being a mixture of different calcium carbonate polymorphs: vaterite, aragonite and calcite, similar to the transformation of the reaction products in OPC as a consequence of carbonation processes [43,44]. In alkali-activated GBFS with $Na_2O{\cdot}rSiO_2$ solutions, natron ($Na_2CO_3 \cdot 10H_2O$) has also been reported as a carbonation product [11,12] but was not observed in the samples assessed here. This distinction is probably due to differences in pore solution chemistry between samples made with slightly different activators and from different slags; the trona or natron are crystallizing from the pore solutions and incorporating the alkali present there, meaning that a more alkaline pore solution will crystallize natron, whereas a less alkaline pore solution will contain more bicarbonate species and so may crystallize trona instead. The pKa of the CO_3^{2-}/HCO_3^- equilibrium is around 10.3, meaning that bicarbonate is only expected to form in significant quantities once carbonation has commenced to such an extent to reduce the pore solution pH to this level. The identification of the pore solution as the source of alkalis for this process is supported by the absence of these phases in the metakaolin-containing sample, where the increased binding of Na^+ into the aluminosilicate (N–A–S–H) gel phases formed in the presence of MK will reduce the driving force for sodium (bi)carbonate precipitation in the pores.

In uncarbonated pastes activated with Ms = 2.0 (Fig. 5A), the same phases previously identified in samples activated with Ms = 2.4 (calcite, quartz, gelhenite, C–S–H gel and gismondine) are observed. However, in this case, the higher alkalinity associated with the lower modulus activator contributes to the formation of an additional reaction product: a sodium–calcium silicate hydrate (Na–C–S–H) ($Na_2Ca_2Si_2O_7 \cdot H_2O$) (PDF# 00-022-0891). After carbonation (Fig. 5B), in binders with GBFS/(GBFS + MK) = 0.9 activated with Ms = 2.0, the Na–C–S–H phase is not identified. This suggests that carbonation could take place initially in the C–S–H gel, forming $CaCO_3$ as a first reaction product. The less-stable (but less prone to decalcification due to its lower Ca content) Na–C–S–H may then break down, with components migrating to balance charges in the decalcified C–S–H gel, instead of forming sodium carbonates. Such a mechanism is of course speculative, but is coherent with the fact that sodium carbonates (natron and/or trona) are not identified in these samples as carbonation products, which is uncommon in carbonated AAS materials.

3.5. Infrared spectroscopy

Uncarbonated pastes with GBFS/(GBFS + MK) = 1.0 and Ms = 2.4 (Fig. 6A) exhibit infrared vibration modes at 1662 cm^{-1} and 1639 cm^{-1} associated with bending vibrations of H–OH bonds, related to water

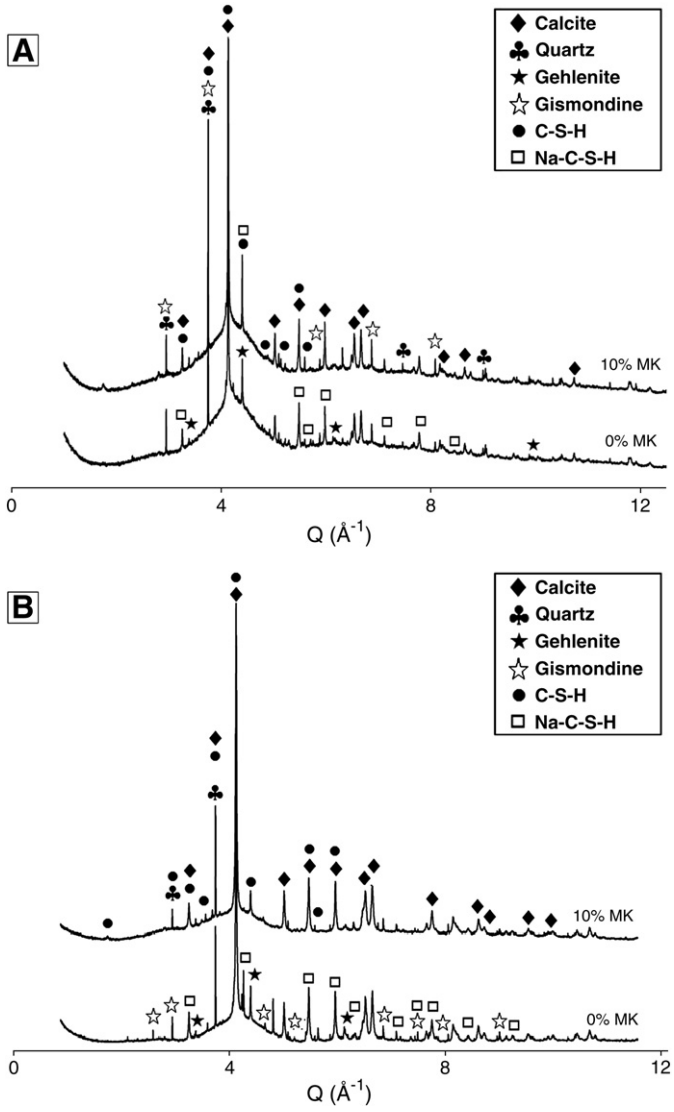

Fig. 5. High resolution synchrotron X-ray diffraction patterns of (A) uncarbonated (λ = 0.401738 Å and (B) carbonated pastes (λ = 0.458879 Å) based on alkali-activated GBFS and GBFS/MK blends with Ms = 2.0.

bound in the hydrated products formed after alkaline activation. A mode at 1438 cm^{-1} corresponding to the stretching vibration of O–C–O bonds in the carbonate group (CO_3^{2-}) was also observed. Carbonates were present in uncarbonated samples due to weathering of the slag before alkaline activation, consistent with the observation of calcite in the XRD data for these samples (Fig. 4A). The mode at 983 cm^{-1} is assigned to the asymmetric stretching vibration of Si–O–T bonds, where T is tetrahedral silicon or aluminum. This specific frequency is characteristic of silicon tetrahedra (SiO_4) in the chain structure of calcium silicate hydrate (C–S–H). The shoulder at 877 cm^{-1} is associated to the asymmetric stretch of AlO_4^- groups, and the mode at 715 cm^{-1} corresponds to the bending of Al–O–Si bonds. These bands have also been identified in unreacted slag [18] and could be related to the gehlenite identified by X-ray diffractometry. All infrared band assignments follow references [45–49].

As a consequence of carbonation of pastes solely based on GBFS (Fig. 6A), the asymmetric stretching vibration of O–C–O bonds of CO_3^{2-} groups shifted slightly (1438 cm^{-1}, to 1417 cm^{-1}), and a marked increase in the intensity of this vibration was observed. The 983 cm^{-1} band shifts to 1001 cm^{-1}, with a significant decrease in its intensity. This indicates chemical changes in the reaction products formed by alkaline activation of the GBFS, in particular the decalcification of the C–S–H gel to form calcium carbonates and amorphous silica [11–13]. An increase in the wavelength of this peak indicates a higher degree of polymerisation of silicates within the remnant gel, as the calcium is removed and Si–O–Si bonds form. An increase in the intensity of the mode between 880 and 870 cm^{-1} is also associated with the formation of calcite; the small peak in this region that is present before carbonation can again be attributed to the weathering of the slag before alkaline activation. A new band at 833 cm^{-1} in the carbonated GBFS sample is assigned to a bending mode in the HCO_3^- ion, which is characteristic of the formation of trona [49] and consistent with the XRD data in Fig. 4.

The incorporation of 10% MK (Fig. 6C) into binders activated with Ms 2.4 leads to a shift in the asymmetric stretching vibration of the Si–O–T bonds to higher wavenumbers (from 983 cm^{-1} in the slag-only sample to 1005 cm^{-1}), indicating that the reaction products in the uncarbonated samples are more highly polymerize as a consequence of the higher Al content leading to condensation of tetrahedral species [32,50]. Carbonation of these samples (Fig. 6D) again leads, as expected, to an increased intensity in the peaks assigned to calcite. A reduction in the intensity of the asymmetric stretching vibration of Si–O–T bonds, accompanied by the formation of a shoulder at 1158 cm^{-1}, was observed. This indicates that carbonation in these pastes is more intense when compared with those based solely on GBFS, coherent with the carbonation depth measurements and changes in compressive strength exhibited by mortars based on this binder. The high-wavenumber shoulder is associated with a reasonably pure and highly-coordinated silica gel phase. Trona (peak at 833 cm^{-1} in the slag-only samples) is not observed in these samples, again consistent with the XRD data.

In uncarbonated slag-only samples with lower Ms (Fig. 6B), the asymmetric stretching vibration of Si–O–T bonds is present at lower wavelengths compared to Ms 2.4 sample, indicating a lower Si content in the C–S–H gels produced in this binder. A small peak at 668 cm^{-1}, attributed to the symmetrical stretching vibration of Si–O–Si or Al–O–Si bonds, was also observed in this sample, and the bending vibration of these same bonds was identified at 457 cm^{-1} [50–52]. The carbonation of these samples leads to a substantial increase in the intensity of the characteristic calcite peaks [46,49]. The development of a small peak in the HCO_3^- region at 836 cm^{-1} is also observed, although no crystalline bicarbonate phases are observed in XRD (Fig. 5), meaning that the bicarbonate ions may either be present in non-crystalline structures or in the pore solution. An increase in the intensity and a shift to higher wavenumber of the modes associated with the symmetrical stretching and bending vibrations of Si–O–T bonds was also identified.

Under these activation conditions (Ms 2.0), the incorporation of MK as a second component in the binder (Fig. 6D) leads to a significant reduction in the intensity of the Si–O–T asymmetric stretching vibration, and its shift to higher wavenumbers compared when with the observed for samples solely formulated with GBFS. The spectrum of this carbonated sample is similar to that which is obtained from carbonated samples when activation is carried out with Ms 2.4 and 10% incorporation of MK.

3.6. Thermogravimetry

Uncarbonated pastes based on GBFS activated with Ms 2.4 and 2.0 show (Fig. 7A; presented as differential thermogravimetry (DTG) data) a mass loss at 60–160 °C, associated with the free and/or loosely bound water present in the samples (Region I) [53,54]. Dehydration of the C–S–H reaction product is identified as a progressive mass loss above 380 °C (region II), consistent with the data of Taylor [34]. The lower-modulus activating solution (data set 3 in Fig. 7A) shows more mass loss in this region, which may be associated with the presence of more chemically bound water (–OH) groups in this sample. No distinct signal due to zeolitic reaction products is observed in any of

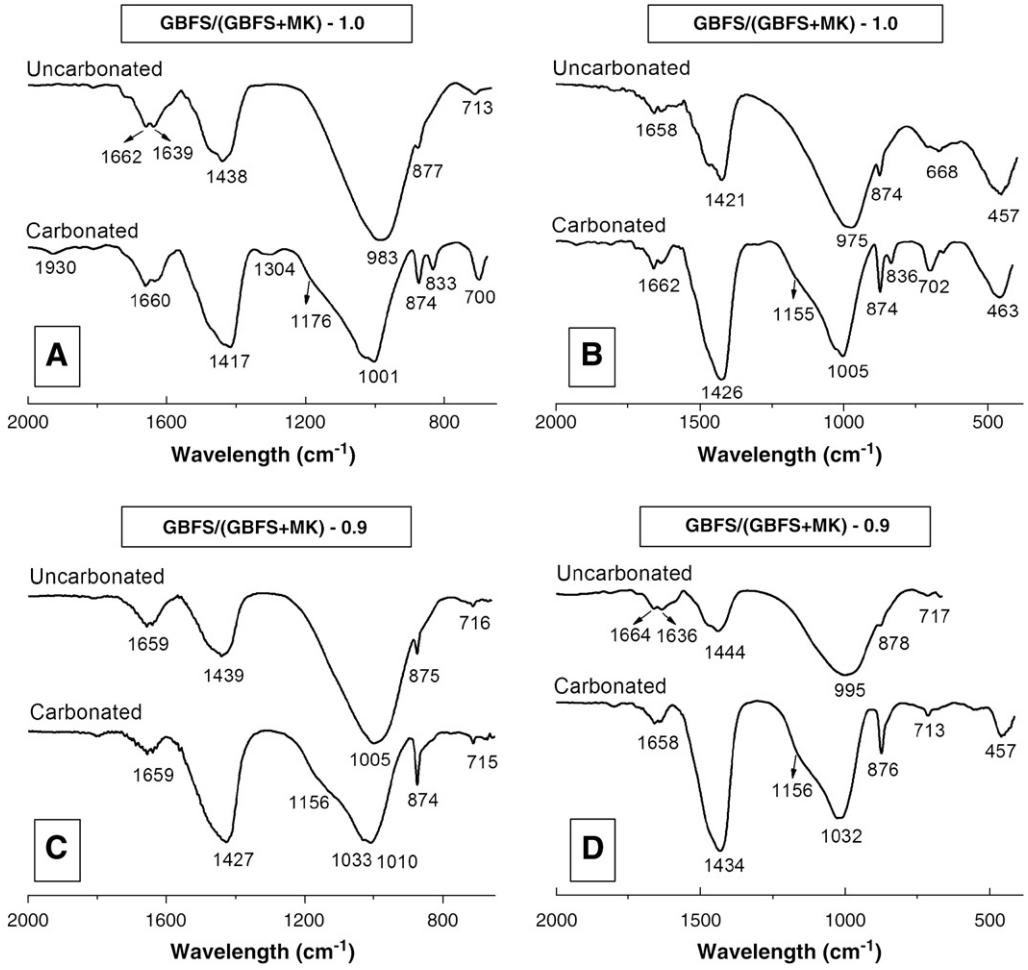

Fig. 6. Fourier transform infrared spectra of uncarbonated and carbonated pastes of (A;B) GBFS and (C;D) GBFS/MK blends, activated with (A;C) Ms = 2.4, (B;D) Ms = 2.0.

the data sets, which is not unexpected as gisnmondine-group zeolites tend to show a broad dehydration peak in this temperature range. There is then a significant peak observed at temperatures between 650 °C and 670 °C in all samples, and smaller peaks between 770 and 790 °C, which are all attributed to the presence of calcium carbonates of varying crystallinity [54,55]. Region III, above 800 °C, shows only a small peak in one sample.

Similar to uncarbonated specimens (Fig. 7A), three regions are identified in the DTA curves of carbonated samples (Fig. 7B). Free and loosely bound water are released below about 160 °C (Region I), and trona degrades in this temperature range also but its signal is dominated by the free water peak. There are only minimal changes in mass above 800 °C (Region III). The major change observed is in Region II, where the mass loss below 600 °C is much greater and the $CaCO_3$ decomposition peak at ~660–680 °C is broadened and more intense. This can be correlated with the presence of much more $CaCO_3$ in the samples, as well as effects in the lower-temperature portion of this region due to the chemically bound water in the silica gel which is

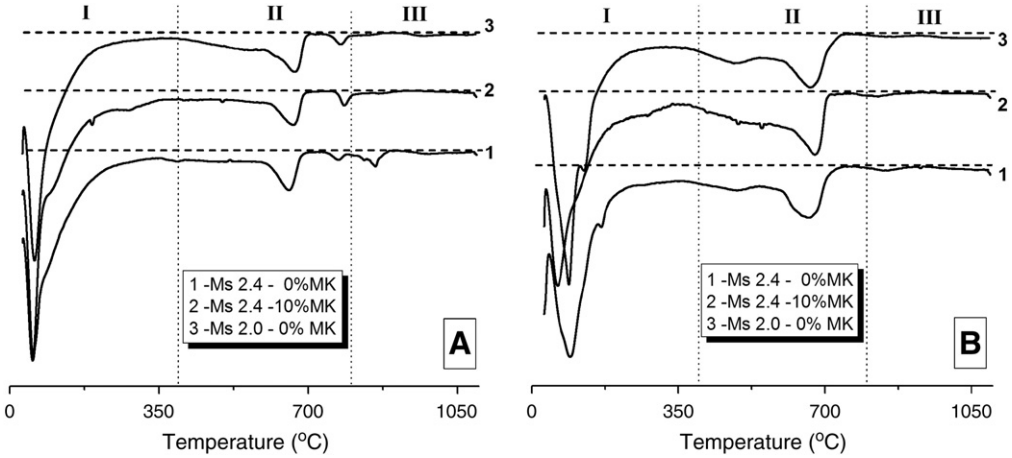

Fig. 7. Differential thermograms (mass loss downwards, dashed lines indicate zero for each data set) of (A) uncarbonated and (B) carbonated pastes based on alkali-activated GBFS/MK blends.

formed by C–S–H decalcification. However, the DTG signals in this region, induced by the presence of the different hydrate and gel phases, all tend to be broad and overlapping.

The relative amounts of carbonates formed in each sample suggest higher calcite content in carbonated pastes with Ms 2.0 than with Ms 2.4. These results are in agreement with the carbonation depth measurements, which show that carbonation is more intense when the activation is carried out at lower Ms. A higher content of calcite in the carbonated samples is indicating an increased extent of reaction between CO_2 and the hydration products obtained in these binders, which correlates well with the substantial increase in capillary sorptivity observed above. This shows that any pore-blocking effects attributable to the deposition of additional $CaCO_3$ are outweighed by the degradation of the microstructure in the more intensely carbonated samples.

4. Conclusions

The mechanism and effects of carbonation in alkali silicate-activated slag and slag/metakaolin blends have been examined. Carbonation is more rapid in samples containing more metakaolin, and the effect of the silicate activator modulus depends on whether or not metakaolin is present — slag-only systems that are more alkaline are also more rapidly carbonated, whereas higher alkalinity in metakaolin-containing systems leads to a higher extent of formation of aluminosilicate binder components and thus reduces the carbonation rate. The presence of gismondine as a zeolitic aluminosilicate reaction product is observed in uncarbonated metakaolin-containing samples.

The main carbonation product in all samples is calcite, with no other calcium carbonate polymorphs observable. Trona is formed in metakaolin-free samples by direct carbonation involving free sodium in the pore solution, but is not formed in samples containing even 10% metakaolin because the aluminosilicate gel present as a secondary alkali-activation product in these materials contributes to the binding of Na^+.

The results of this study run contrary to some claims in the literature that alkali-activated binders are on the whole highly resistant to carbonation. It is intriguing to note that these materials do tend to perform poorly in accelerated tests but have been reported to show acceptable durability in service, and developing a more detailed mechanistic understanding of the process of carbonation is certainly critical to understanding this discrepancy.

Acknowledgements

This study was sponsored by the *Universidad del Valle* (Colombia), *Instituto Colombiano para el Desarrollo de la Ciencia y Tecnología "Francisco José de Caldas"* (COLCIENCIAS) and the Center of Excellence of Novel Materials (CENM). We would like to thank Carmen Elisa Guerrero for the assistance with thermogravimetry. Use of the Advanced Photon Source at Argonne National Laboratory was supported by the U. S. Department of Energy, Office of Science, Office of Basic Energy Sciences, under Contract No. DE-AC02-06CH11357. The participation of JLP was funded by the Australian Research Council (ARC), including partial funding through the Particulate Fluids Processing Centre, a Special Research Centre of the ARC.

References

[1] D.W. Hobbs, Concrete deterioration: causes, diagnosis, and minimising risk, Int. Mater. Rev. 46 (3) (2001) 117–144.
[2] A. Poonguzhali, H. Shaikh, R.K. Dayal, H.S. Khatak, Degradation mechanism and life estimation of civil structures — a review, Corros. Rev. 26 (4) (2008) 215–294.
[3] F.P. Glasser, J. Marchand, E. Samson, Durability of concrete — degradation phenomena involving detrimental chemical reactions, Cem. Concr. Res. 38 (2) (2008) 226–246.
[4] C. Andrade, Seminario S.3: Patología del Hormigón, Durabilidad (Corrosión), *X Curso de Estudios Mayores de la Construcción*, Edificación, Su Patología y Control de Calidad — CEMCO *85*, Madrid, Spain, 1985.
[5] A. Steffens, Modeling carbonation for corrosion risk prediction of concrete structures, Cem. Concr. Res. 32 (2002) 938–941.
[6] V.G. Papadakis, C.G. Vayenas, M.N. Fardis, Experimental investigation and mathematical modeling of the concrete carbonation problem, Chem. Eng. Sci. 46 (1991) 1333–1338.
[7] B. Johannesson, P. Utgenannt, Microstructural changes caused by carbonation of cement mortar, Cem. Concr. Res. 31 (2001) 925–931.
[8] M. Castellote, L. Fernandez, C. Andrade, C. Alonso, Chemical changes and phase analysis of OPC pastes carbonated at different CO_2 concentrations, Mater. Struct. 42 (2009) 515–525.
[9] K. Byfors, V. Klingstedt, P.Y.Y. Lehtonen, L. Rombern, Durability of concrete made with alkali activated slag, Proceedings of the 3th International Conference on Fly Ash, Silica Fume, Slag and Natural Pozzolans in Concrete, American Concrete Institute, Trondheim, Norway, 1989.
[10] T. Bakharev, J.G. Sanjayan, Y.B. Cheng, Resistance of alkali-activated slag concrete to carbonation, Cem. Concr. Res. 31 (2001) 1277–1283.
[11] F. Puertas, M. Palacios, T. Vázquez, Carbonation process of alkali-activated slag mortars, J. Mater. Sci. 41 (2006) 3071–3082.
[12] M. Palacios, F. Puertas, Effect of carbonation on alkali-activated slag paste, J. Am. Ceram. Soc 89 (10) (2006) 3211–3221.
[13] S.A. Bernal, E. Rodríguez, R. Mejía de Gutiérrez, V. Rose, F. Puertas, S. Delvasto, Carbonation behavior of mortar produced by alkali-activation of a granulated-blast furnace slag, Proceedings of 23 rd International Conference on Solid Waste Technology and Management, Widener University, Philadelphia, PA, 2008.
[14] J. Deja, Carbonation aspects of alkali activated slag mortars and concretes, Silic. Ind. 67 (1) (2002) 37–42.
[15] H. Xu, J.L. Provis, J.S.J. van Deventer, P.V. Krivenko, Characterization of aged slag concretes, ACI Mater. J. 105 (2) (2008) 131–139.
[16] C.K. Yip, J.S.J. van Deventer, Microanalysis of calcium silicate hydrate gel formed within a geopolymeric binder, J. Mater. Sci. 38 (18) (2003) 3851–3860.
[17] C.K. Yip, G.C. Lukey, J.L. Provis, J.S.J. van Deventer, Effect of calcium silicate sources on geopolymerisation, Cem. Concr. Res. 38 (4) (2008) 554–564.
[18] S.A. Bernal, Ph.D. Thesis, Universidad del Valle, Cali, Colombia, 2009.
[19] G. Fagerlund, On the capillarity of concrete, Nord Concr. Res. 1 (1982) 6.1–6.20.
[20] F. Collins, J.G. Sanjayan, Microcracking and strength development of alkali activated slag concrete, Cem. Concr. Compos. 23 (2001) 345–352.
[21] E. Rodríguez, R. Mejía de Gutiérrez, S.A. Bernal, F. Puertas, M. Gordillo, S. Delvasto, Resistencia química de morteros de escoria siderúrgica activada alcalinamente, Proceedings of the International Conference on Non-Conventional Materials and Technologies — NOCMAT, Maceió, Brazil, 2007.
[22] C. Shi, Corrosion resistance of alkali-activated slag cement, Adv. Cem. Res. 15 (2) (2003) 77–81.
[23] H. Zhou, X. Wu, Z. Xu, M. Tang, Kinetic study on hydration of alkali-activated slag, Cem. Concr. Res. 23 (1993) 1253–1258.
[24] S.D. Wang, K.L. Scrivener, Hydration products of alkali-activated slag cement, Cem. Concr. Res. 25 (3) (1995) 561–571.
[25] F. Puertas, Cementos de escoria activados alcalinamente: situación actual y perspectivas de futuro, Mater. Constr. 45 (239) (1995) 53–64.
[26] C. Shi, Early hydration and microstructure development of alkali-activated slag cement pastes, Proceedings of the 10th International Congress on the Chemistry of Cement, Gothenburg, Sweden, 1997, p. 3ii099.
[27] A.R. Brough, A. Atkinson, Sodium silicate-based, alkali-activated slag mortars. Part I. Strength, hydration and microstructure, Cem. Concr. Res. 32 (2002) 865–879.
[28] F. Bonk, J. Schneider, M.A. Cincotto, H. Panepucci, Characterization by multinuclear high-resolution NMR of hydration products in activated blast-furnace slag pastes, J. Am. Ceram. Soc 86 (10) (2003) 1712–1719.
[29] J. Escalante-Garcia, A.F. Fuentes, A. Gorokhovsky, P.E. Fraire-Luna, G. Mendoza-Suarez, Hydration products and reactivity of blast-furnace slag activated by various alkalis, J. Am. Ceram. Soc 86 (12) (2003) 2148–2153.
[30] I.G. Richardson, A.R. Brough, G.W. Groves, C.M. Dobson, The characterization of hardened alkali-activated blast-furnace slag pastes and the nature of the calcium silicate hydrate (C–S–H) paste, Cem. Concr. Res. 24 (5) (1994) 813–829.
[31] A. Fernández-Jiménez, F. Puertas, Setting of alkali-activated slag cement. Influence of activator nature, Adv. Cem. Res. 13 (3) (2001) 115–121.
[32] A. Fernández-Jiménez, F. Puertas, Structure of calcium silicate hydrates formed in alkaline-activated slag: influence of the type of alkaline activator, J. Am. Ceram. Soc 86 (8) (2003) 1389–1394.
[33] Y.J. Zhang, Y.L. Zhao, H.H. Li, D.L. Xu, Structure characterization of hydration products generated by alkaline activation of granulated blast furnace slag, J. Mater. Sci. 43 (2008) 7141–7147.
[34] H.F.W. Taylor, Cement Chemistry, 2nd Ed.Thomas Telford, London, UK, 1997.
[35] J.L. Provis, V. Rose, S.A. Bernal, J.S.J. van Deventer, High resolution nanoprobe X-ray fluorescence characterization of heterogeneous calcium and heavy metal distributions in alkali activated fly ash, Langmuir 25 (19) (2009) 11897–11904.
[36] I.G. Richardson, Tobermorite/jennite- and tobermorite/calcium hydroxide-based models for the structure of C–S–H: applicability to hardened pastes of tricalcium silicate, β-dicalcium silicate, Portland cement, and blends of Portland cement with blast-furnace slag, metakaolin, or silica fume, Cem. Concr. Res. 34 (9) (2004) 1733–1777.
[37] S.-D. Wang, K.L. Scrivener, ^{29}Si and ^{27}Al NMR study of alkali-activated slag, Cem. Concr. Res. 33 (5) (2003) 769–774.
[38] A. Fernández-Jiménez, M. Monzó, M. Vicent, A. Barba, A. Palomo, Alkaline activation of metakaolin-fly ash mixtures: obtain of Zeoceramics and Zeocements, Microporous Mesoporous Mater. 108 (1–3) (2008) 41–49.

[39] M. Criado, A. Palomo, A. Fernández-Jiménez, Alkali activation of fly ashes. Part 1: Effect of curing conditions on the carbonation of the reaction products, Fuel 84 (16) (2005) 2048–2054.
[40] R.R. Lloyd, Ph.D. Thesis, University of Melbourne, Australia, 2008.
[41] J.L. Provis, G.C. Lukey, J.S.J. van Deventer, Do geopolymers actually contain nanocrystalline zeolites? A reexamination of existing results, Chem. Mater. 17 (12) (2005) 3075–3085.
[42] V.D. Glukhovsky, Ancient, modern and future concretes, in: P.V. Krivenko (Ed.), Proceedings of the First International Conference on Alkaline Cements and Concretes, VIPOL Stock Company, Kiev, Ukraine, 1994, pp. 1–9.
[43] E.T. Stepkowska, Hypothetical transformation of $Ca(OH)_2$ into $CaCO_3$ in solid-state reactions of Portland cement, J Therm Anal Calorim 80 (2005) 727–733.
[44] E.T. Stepkowska, M.A. Aviles, J.M. Blanes, J.L. Pérez-Rodríguez, Gradual transformation of $Ca(OH)_2$ into $CaCO_3$ on cement hydration. XRD study, J. Therm. Anal. Calorim. 87 (1) (2007) 189–198.
[45] V.C. Farmer, The Infrared Spectra of Minerals, Mineralogical Society, London, 1974.
[46] J.A. Gadsden, Infrared spectra of minerals and related inorganic compounds, Butterworths, London, 1975.
[47] M. Sitarz, M. Handke, W. Mozgawa, Identification of silicooxygen rings in SiO_2 based on IR spectra, Spectrochim. Acta A 56 (2000) 1819–1823.
[48] M. Sitarz, M. Handke, W. Mozgawa, E. Galuskin, I. Galuskina, The non-ring cations influence on silicooxygen ring vibrations, J. Mol. Struct. 555 (2000) 357–362.
[49] C.K. Huang, P.F. Kerr, Infrared study of the carbonate minerals, Am. Miner. 45 (2) (1960) 311–324.
[50] P. Yu, R.J. Kirkpatrick, B. Poe, P.F. McMillan, X. Cong, Structure of calcium silicate hydrate (C–S–H): near-, mid-, and far-infrared spectroscopy, J. Am. Ceram. Soc 82 (3) (1999) 742–748.
[51] W.K.W. Lee, J.S.J. van Deventer, Use of infrared spectroscopy to study geopolymerization of heterogeneous amorphous aluminosilicates, Langmuir 19 (21) (2003) 8726–8734.
[52] D.W. Breck, Zeolite Molecular Sieves: Structure, Chemistry and Use, Wiley-Interscience, New York, 1974.
[53] V.S. Ramachandran, R.M. Paroli, J.J. Beaudoin, A.H. Delgado, Handbook of Thermal Analysis of Construction Materials, Noyes Publication/William Andrew Publishing, Norwich, NY, 2003.
[54] A. Hidalgo, C. Domingo, C. Garcia, S. Petit, C. Andrade, C. Alonso, Microstructural changes induced in Portland cement-based materials due to natural and supercritical carbonation, J. Mater. Sci. 43 (2008) 3101–3111.
[55] L. Haselbach, Potential for carbon dioxide absorption in concrete, J. Environ. Eng. 135 (6) (2009) 465–472.